

Joint User Identification, Channel Estimation, and Signal Detection for Grant-Free NOMA

Shuchao Jiang, Xiaojun Yuan, Xin Wang, Chongbin Xu, and Wei Yu

Abstract

For massive machine-type communications, centralized control may incur a prohibitively high overhead. Grant-free non-orthogonal multiple access (NOMA) provides possible solutions, yet poses new challenges for efficient receiver design. In this paper, we develop a joint user identification, channel estimation, and signal detection (JUICESD) algorithm. Specifically, we divide the whole detection scheme into linear and non-linear modules. Then we handle the linear module by leveraging the existing approximate message passing (AMP) algorithms, and deal with the non-linear module based on generalized messaging passing. The exact calculation of the messages exchanged within the non-linear module and between the two modules is complicated due to phase ambiguity issues. By noticing that the messages under phase ambiguity exhibit a rotational invariance property, we propose a rotationally invariant Gaussian mixture (RiGm) model, and develop an efficient JUICESD-RiGm algorithm. JUICESD-RiGm achieves a performance close to JUICESD with a much lower complexity. Capitalizing on the feature of RiGm, we further analyze the performance of JUICESD-RiGm with state evolution techniques. Numerical results demonstrate that the proposed algorithms achieve a significant performance improvement over the existing alternatives, and even outperform oracle linear minimum mean square error (LMMSE) receivers; and the derived state evolution method predicts the system performance accurately.

Index Terms

Grant-free NOMA, AMP, rotationally invariant Gaussian mixture (RiGm), state evolution

This paper will be presented in part at IEEE GLOBECOM 2019, Hawaii, USA, December 2019 [38].

Shuchao Jiang, Xin Wang, and Chongbin Xu are with the Key Laboratory for Information Science of Electromagnetic Waves (MoE), Shanghai Institute for Advanced Communication and Data Science, Department of Communication Science and Engineering, Fudan University, Shanghai 200433, China (e-mail: {17110720042, xwang11, chbinxu}@fudan.edu.cn).

Xiaojun Yuan is with the Center for Intelligent Networking and Communication (CINC), University of Electronic Science and Technology of China, Chengdu 610000, China (e-mail: xjyuan@uestc.edu.cn).

Wei Yu is with the Department of Electrical and Computer Engineering, University of Toronto, Toronto, Ontario M5S 3G4, Canada (e-mail: weiyu@comm.utoronto.ca).

I. INTRODUCTION

Massive machine-type communication (mMTC) is one of the most important scenarios for the next generation communications [1], [2]. It is a key technology for realizing large-scale Internet of Things (IoT) applications such as smart home, smart manufacturing, and smart health care, etc. Different from conventional human-type communications, an mMTC scenario may involve a huge number of users. The packet arrival rate of each user can be low and the packet length is typically short [3]. In this case, the multiple access protocol plays a key role in supporting the massive connectivity efficiently [4], [5]. Due to the large signaling overhead, the conventional centralized control based multiple access techniques, e.g., orthogonal frequency division multiplexing and time division multiple access, are generally not desirable.

Grant-free non-orthogonal multiple access (NOMA) has been proposed [6]–[8] to reduce signaling overhead and enhance access capability. In grant-free NOMA, time and/or frequency domain resource blocks are divided into non-orthogonal sub-blocks that are shared by all potential users; and active users freely access the channel without waiting for any scheduling grant. This significantly reduces the overhead of control signaling to meet the requirement of mMTC.

Grant-free NOMA, however, poses a challenge for reliable receiver design. Besides channel estimation and signal detection, the receiver also needs to identify the activities of all potential users (i.e., which users simultaneously transmit packets) since there is no scheduling information at the receiver. A straightforward approach to the receiver design is first to identify active users, then to estimate the channel coefficients of the active users, and finally to recover the data of the active users. However, this separate processing approach may consume a substantial amount of spectrum and power resource, which in turn degrades the system performance.

For the sparse signal recovery problem involved in the receiver design of grant-free NOMA, compressed sensing (CS) [9] has been widely used. A possible approach for solving the CS problem is the l_1 -norm relaxation via convex programming [10]. However, the complexity of convex programming is high, especially for recovering high-dimensional signals. Other approximate algorithms have been proposed for more efficient sparse signal recovery, including match pursuit [11], orthogonal match pursuit [12], iterative soft thresholding [13], compressive sampling matching pursuit [14], approximate message passing (AMP) [15] and its variants [16]–[23]. In particular, AMP provides a low-cost yet asymptotically optimal solution for a linear system with an independent and identically distributed (i.i.d.) sensing matrix [15], and its performance can

be accurately characterized by the state evolution [24]. Furthermore, sparse signal recovery algorithms for more general system models have been developed recently, including turbo compressed sensing [16], orthogonal AMP (OAMP) [17] and vector AMP (VAMP) [18] for linear systems with a non-i.i.d. sensing matrix, generalized AMP (GAMP) [20], [21] for systems with non-linear output, and bilinear GAMP (BiGAMP) [22], [23] for bi-linear systems. These message passing based algorithms provide the current state of the art for sparse signal reconstruction.

Based on aforementioned algorithms, joint designs of channel estimation, user identification, and/or signal detection have been pursued to improve the system performance. Specifically, under the assumption of perfect channel state information (CSI) at the receiver (CSIR), joint active user identification and signal detection algorithms were developed in [25], [26]. For systems without CSIR, [27]–[30] established joint channel estimation and active user identification algorithms, followed by separated signal detection operations. In addition, joint channel and data estimation algorithms were developed for massive MIMO systems [31]–[34] and for single carrier systems [35].

Recently, [36] proposed a joint channel estimation and multiuser detection algorithm, named block sparsity adaptive subspace pursuit (BSASP). This algorithm transfers the single-measurement-vector compressive sensing (SMV-CS) problem to multiple-measurement-vector compressive sensing (MMV-CS), and reconstructs the sparse signal by exploiting the inherent block sparsity of the channel. BSASP generally suffers from the non-orthogonality of the training matrix. This issue becomes more serious in massive connectivity case, since the non-orthogonal training is usually inevitable in order to accommodate as many potential users as possible. In [37], a message-passing based joint channel estimation and data decoding algorithm was proposed for grant-free sparse code multiple access (SCMA) systems, where the messages were approximated by Gaussian distributions with minimized Kullback-Leibler (KL) divergence.

In this paper, we develop a joint user identification, channel estimation, and signal detection (JUICESD) algorithm based on message passing principles for grant-free NOMA systems. For this joint detection problem, the channel coefficients, the user activity states, and the transmit signals are coupled together, forming a complicated tri-linear signal model to which the existing AMP algorithms (mostly developed for linear models) cannot be applied directly. Existing works mainly focus on some simplified signal models and only solve the problem partially, e.g., by assuming that the CSI is perfectly known at the receiver [25], [26], or by dividing the whole scheme into two phases, i.e., one phase for joint channel estimation and active user identification,

and the other for separated signal detection [27]–[29]. Different from the existing approaches, the main contributions of this paper include the following three aspects:

- By introducing appropriate auxiliary variables, we divide the whole tri-linear signal detection scheme into a linear module and a non-linear module. Then, for the linear module, an AMP-type algorithm is developed to leverage the low complexity and the asymptotic optimality of AMP. The non-linear module can be decoupled for different users, and a generalized message passing algorithm is derived in a user-by-user fashion. The overall algorithm, termed the JUICESD algorithm, is thus developed. It is shown that JUICESD achieves a significant performance improvement over the existing alternatives, and can even outperform linear minimum mean square error (LMMSE) receivers with oracle user activity information.
- The exact calculation of the messages exchanged within the non-linear module and between the two modules in JUICESD involves computational complexity exponential in the frame length. To reduce computational complexity, we show that the messages in the JUICESD algorithm exhibit a rotational invariance property. We thus propose a rotationally invariant Gaussian mixture (RiGm) model for the message updates, and develop an efficient JUICESD-RiGm algorithm. JUICESD-RiGm achieves a performance close to JUICESD but with a much lower complexity that is quadratic in the frame length. Hence, it is well suited for machine type communications with massive devices and short packets.
- Capitalizing on the feature of the proposed RiGm model, we further analyze the performance of JUICESD-RiGm by developing a state evolution technique. Numerical results show that the derived state evolution method predicts the system performance accurately. This analysis may provide useful insights for future system design and optimization.

The rest of this paper is organized as follows. Section II outlines the system model and formulates the problem of interest. Section III develops the JUICESD algorithm, while Section IV proposes the JUICESD-RiGm algorithm. The performance of JUICESD-RiGm is characterized by using state evolution techniques in Section V. Numerical results are provided in Section VI. Section VII concludes the paper.

Notation: We use boldface uppercase letters such as \mathbf{A} to denote matrices, and use boldface lowercase letters such as \mathbf{b} to denote vectors; \mathbf{a}_k denotes the k -th column of matrix \mathbf{A} , $a_{l,k}$ denotes the entry in the l -th row and k -th column of matrix \mathbf{A} ; and b_k denotes the k -th element of vector \mathbf{b} . For matrices and vectors, $(\cdot)^T$ denotes transpose, $\text{diag}(\mathbf{b})$ is the diagonal matrix

with the diagonal elements specified by \mathbf{b} . Denote by \mathcal{A} a set, and by $|\mathcal{A}|$ the cardinality of \mathcal{A} ; $\mathcal{N}(\mu, \tau)$ denotes the Gaussian distribution with mean μ and variance τ ; $\mathcal{CN}(\mu, \tau)$ denotes the complex Gaussian distribution with mean μ , variance τ , and zero relation.

II. SYSTEM MODEL

Consider a typical mMTC scenario, in which a large number of users with sporadic traffic communicate with a single access point (AP). Based on the received signals, the AP is responsible for judging which users are active, estimating the channels of the active users, and recovering the signals transmitted by the active users.

A. Grant-Free NOMA Transmission

We follow the spreading based NOMA schemes in [25], [26], [36] for grant-free transmissions. Specifically, each user k is assigned with a unique spreading sequence $\mathbf{a}_k = [a_{1,k}, \dots, a_{L,k}]^T$ as its signature, where L is the spreading length. For massive connectivity case, L can be much less than the total number of users K , and therefore orthogonal spreading sequence design is generally impossible. Here we assume that the elements of each \mathbf{a}_k are randomly and independently drawn from the Gaussian distribution $\mathcal{N}(0, 1/L)$ [17], [24].

Consider the transmission in a frame of T slots, where each slot consists of L transmission symbols corresponding to the length of the spreading sequence. The received signal can be modeled as [36], [38]

$$\mathbf{r}_t = \sum_{k=1}^K \mathbf{a}_k h_k u_k x_{k,t} + \mathbf{w}_t, \quad t = 1, \dots, T \quad (1)$$

where K is the total number of users, h_k is the channel coefficient from user k to the AP, u_k is an indicator to represent the activity state of user k (with $u_k = 1$ meaning that user k is active and $u_k = 0$ otherwise), $x_{k,t}$ is the transmit signal of user k at time slot t , and each entry of \mathbf{w}_t is the complex additive white Gaussian noise (AWGN) with mean zero and variance N_0 . All $\{h_k\}$, $\{u_k\}$, and $\{x_{k,t}\}$ are assumed to be independently distributed.

Block fading is assumed, i.e., h_k and u_k remain unchanged within each transmission frame. The channel coefficient h_k is modelled as $h_k = \sqrt{\beta_k} \alpha_k$, $\forall k$, where $\alpha_k \sim \mathcal{CN}(0, 1)$ denotes the Rayleigh fading component, and β_k denotes large scale fading component including path-loss and shadowing. Then we have $h_k \sim p_{H_k}(h_k) = \mathcal{CN}(0, \beta_k)$.

The user symbols $\{x_{k,t}\}$ are modulated by using a common signal constellation \mathcal{S} with cardinality $|\mathcal{S}|$, i.e., each $x_{k,t}$ is randomly and uniformly drawn from \mathcal{S} . We say that \mathcal{S} is

rotationally invariant with respect to a phase shift θ if $\mathcal{S} = e^{j\theta}\mathcal{S}$. Define by $\Omega_{\mathcal{S}}$ the set of all rotationally invariant phase shifts of \mathcal{S} in the range $(0, 2\pi]$. By noting that $\Omega_{\mathcal{S}}$ is a cyclic group under addition, we can generally express $\Omega_{\mathcal{S}}$ as $\Omega_{\mathcal{S}} = \{\theta_0, 2\theta_0, \dots, |\Omega_{\mathcal{S}}|\theta_0\}$, where θ_0 is the minimum value in $\Omega_{\mathcal{S}}$. Such a rotational invariance property holds for commonly used modulation schemes such as phase shift keying (PSK) and quadrature amplitude modulation (QAM), and will be utilized later in the algorithm design in Section IV. Fig. 1 shows the example of the standard 16QAM where $\mathcal{S} = \frac{1}{\sqrt{10}}\{x_r + jx_i \mid x_r, x_i \in \{-3, -1, 1, 3\}\}$, and $\Omega_{\mathcal{S}} = \{0.5\pi, \pi, 1.5\pi, 2\pi\}$.

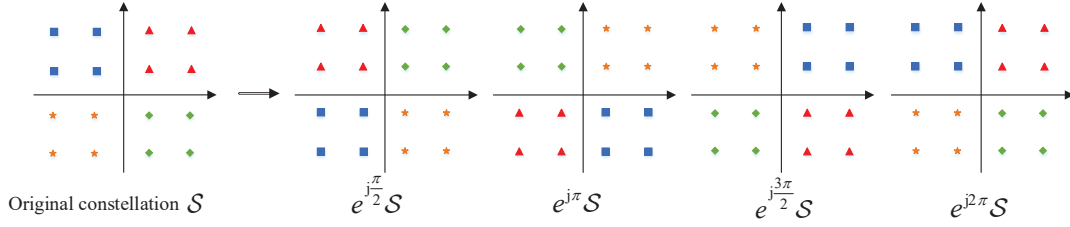


Fig. 1. Rotational invariance of the standard 16QAM constellation.

Throughout the paper, we make the following assumptions [34], [36].

- All users are synchronized in frames. This can be achieved by the AP sending a beacon signal to initialize uplink transmissions [1], [8].
- The packet arrival rate of each user per frame is Bernoulli distributed with parameter $\lambda \in (0, 1]$. Each user starts to transmit a packet at the beginning of a frame with probability λ .
- Retransmissions are not considered and all packets are regarded as new arrivals.

B. Problem Formulation

The focus of this paper is the design of an efficient receiver to identify the activity of all potential users, to estimate the channel coefficients, and to recover the transmit data of the active users. To this end, we rewrite the received signal (1) as

$$\mathbf{R} = \mathbf{A}\mathbf{H}\mathbf{U}\mathbf{X} + \mathbf{W} \quad (2)$$

where $\mathbf{R} = [\mathbf{r}_1, \dots, \mathbf{r}_T] \in \mathbb{C}^{L \times T}$, $\mathbf{A} = [\mathbf{a}_1, \dots, \mathbf{a}_K] \in \mathbb{R}^{L \times K}$, $\mathbf{H} = \text{diag}([h_1, \dots, h_K]^T) \in \mathbb{C}^{K \times K}$, $\mathbf{U} = \text{diag}([u_1, \dots, u_K]^T) \in \{0, 1\}^{K \times K}$, $\mathbf{X} = [x_{k,t}] \in \mathcal{S}^{K \times T}$, and $\mathbf{W} = [\mathbf{w}_1, \dots, \mathbf{w}_T] \in \mathbb{C}^{L \times T}$.

Suppose that the AP jointly estimates $(\mathbf{H}, \mathbf{U}, \mathbf{X})$ by following the maximum *a-posteriori* probability (MAP) principle. Conditioned on \mathbf{R} , the *a-posteriori* probability density function (PDF) is given by

$$\begin{aligned}
p_{H,U,X|R}(\mathbf{H}, \mathbf{U}, \mathbf{X} | \mathbf{R}) &\propto p_{R|H,U,X}(\mathbf{R} | \mathbf{H}, \mathbf{U}, \mathbf{X}) p_H(\mathbf{H}) p_U(\mathbf{U}) p_X(\mathbf{X}) \\
&\propto \exp\left(-\frac{\|\mathbf{R} - \mathbf{A}\mathbf{H}\mathbf{U}\mathbf{X}\|_F^2}{N_0}\right) p_H(\mathbf{H}) p_U(\mathbf{U}) p_X(\mathbf{X})
\end{aligned} \tag{3}$$

where the channel coefficient h_k is drawn from $\mathcal{CN}(0, \beta_k)$; the activity indicator u_k is drawn from the Bernoulli distribution $p_u(u_k) = (1-\lambda)\delta(u_k) + \lambda\delta(u_k-1)$; the elements of \mathbf{X} are independently drawn from a uniform distribution over the signal constellation \mathcal{S} , i.e., $p_S(s) = \frac{1}{|\mathcal{S}|} \sum_{j=1}^{|\mathcal{S}|} \delta(s-s_j)$ with $\sum_{j=1}^{|\mathcal{S}|} \|s_j\|^2/|\mathcal{S}| = 1$ for power normalization.

Based on (3), the MAP estimate of $(\mathbf{H}, \mathbf{U}, \mathbf{X})$ is given by

$$(\hat{\mathbf{H}}, \hat{\mathbf{U}}, \hat{\mathbf{X}}) = \arg \max_{(\mathbf{H}, \mathbf{U}, \mathbf{X})} \exp\left(-\frac{\|\mathbf{R} - \mathbf{A}\mathbf{H}\mathbf{U}\mathbf{X}\|_F^2}{N_0}\right) p_H(\mathbf{H}) p_U(\mathbf{U}) p_X(\mathbf{X}). \tag{4}$$

The solution to problem (4) is not unique. For example, let $\mathbf{D} = \text{diag}([e^{-j\theta_1}, \dots, e^{-j\theta_K}]^T)$ with $\theta_k \in \Omega_S$, $k = 1, 2, \dots, K$. Then, from the rotational invariance property of the constellation \mathcal{S} , we see that $\mathbf{D}\mathbf{X}$ has the same distribution as \mathbf{X} does. Besides, $\mathbf{H}\mathbf{D}^{-1}$ has the same distribution as \mathbf{H} does, which is true for almost all the existing wireless random channel models. Thus, if $(\hat{\mathbf{H}}, \hat{\mathbf{U}}, \hat{\mathbf{X}})$ is a solution to problem (4), then $(\hat{\mathbf{H}}\mathbf{D}^{-1}, \hat{\mathbf{U}}, \mathbf{D}\hat{\mathbf{X}})$ is also a valid solution to problem (4). This phenomenon is referred to as the phase ambiguity of problem (4), which appears widely when data and channels need to be estimated jointly. To remove the phase ambiguity, a simple approach is to insert reference symbols at the first (or any other) column of \mathbf{X} , i.e., each user needs at least one reference symbol for elimination of phase ambiguity. Interestingly, we will show that this “frugal” setting, i.e., one reference symbol per user, is enough to provide accurate channel estimates for our algorithm.

Problem (4) is non-convex and generally difficult to solve. Message passing algorithms could provide possible solutions. However, the variables to be estimated in (4), i.e., \mathbf{H} , \mathbf{U} , and \mathbf{X} , are all coupled to form a tri-linear function. Exact message passing based on the sum-product rule is too complicated to implement, while the existing low complexity AMP-type algorithms [15]–[23] cannot be applied to the tri-linear model in (2) directly. To bypass the dilemma, we next develop a low-complexity yet near-optimal iterative algorithm to solve the problem by a judicious design of the receiver structure and the message updates.

III. PROPOSED JUICESD ALGORITHM

To facilitate a low-complexity yet efficient solution to the joint detection problem in (4), we divide the whole detection scheme into a linear module and a non-linear module by introducing

appropriate auxiliary variables, based on which we develop the proposed JUICESD algorithm.

A. JUICESD Algorithm Structure

Introduce the following auxiliary variables:

$$g_k \doteq h_k u_k, \quad \forall k. \quad (5)$$

$$y_{k,t} \doteq g_k x_{k,t}, \quad \forall k, t. \quad (6)$$

We henceforth refer to g_k and $y_{k,t}$ as the effective channel of user k and the effective signal of user k at time slot t , respectively. Based on the *a-priori* distributions of h_k , u_k , and $x_{k,t}$, we obtain the *a-priori* distributions of g_k and $y_{k,t}$ from (5) and (6) respectively as

$$p_{G_k}(g_k) = (1 - \lambda)\delta(g_k) + \lambda p_{H_k}(g_k), \quad (7)$$

$$p_{y_{k,t}}(y_{k,t}) = (1 - \lambda)\delta(y_{k,t}) + \frac{\lambda}{|\mathcal{S}|} \sum_{j=1}^{|\mathcal{S}|} p_{H_k}(y_{k,t}/s_j). \quad (8)$$

Rewrite the system model in (1) as

$$\mathbf{r}_t = \sum_{k=1}^K \mathbf{a}_k y_{k,t} + \mathbf{w}_t, \quad t = 1, \dots, T. \quad (9)$$

Clearly, the signal model (9) is linear in the auxiliary variables $\{y_{k,t}\}$ since $\{\mathbf{a}_k\}$ are known to the receiver. In addition, given $\{y_{k,t}\}$, the estimations of $\{g_k\}$ and $\{x_{k,t}\}$ are non-linear yet decoupled for different k . These two properties are of importance to our algorithm design.

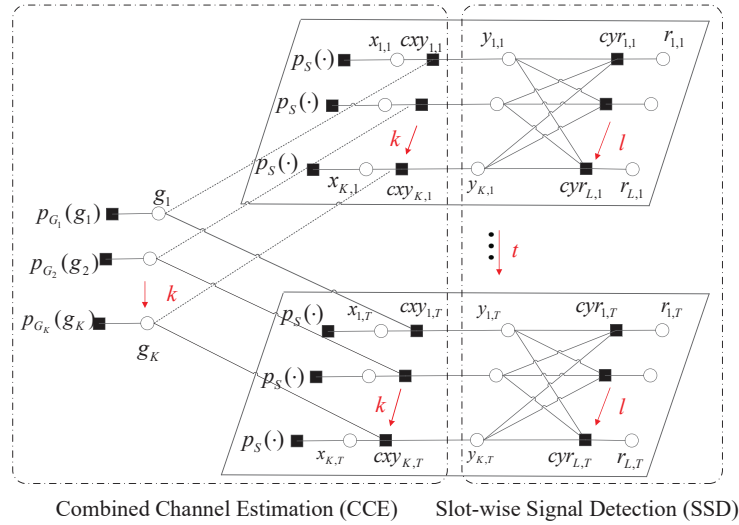


Fig. 2. Factor graph representation of the considered system.

With (6)-(9), we can represent the system model by the factor graph in Fig. 2. The factor graph consists of two types of nodes:

- Variable nodes $\{g_k\}, \{x_{k,t}\}, \{y_{k,t}\}$, and $\{r_{l,t}\}$, depicted as white circles in Fig. 2, corresponding to the variables in (6) and (9), where $r_{l,t}$ is the l -th entry of \mathbf{r}_t ;
- Check nodes $\{p_{G_k}(g_k)\}, p_S(\cdot), \{cxy_{k,t}\}$, and $\{cyr_{l,t}\}$, depicted as black boxes in Fig. 2, corresponding to the marginal *a-priori* distributions of $\{g_k\}$, the marginal *a-priori* distributions of $\{x_{k,t}\}$, the equality constraints in (6), and the equality constraints in (9), respectively.

A variable node is connected to a check node when the variable is involved in the check constraint.

As shown in Fig. 2, we divide the whole receiver structure into two modules, one for the linear signal model in (9) and the other for the non-linear equality constraint in (6). We next outline their main functionalities.

The module on the right hand side of Fig. 2 focuses on the linear signal model in (9). With the messages of $\{y_{k,t}\}$ fed back from the other module as the *a-priori*, the estimation of $\{y_{k,t}\}$ given \mathbf{r}_t in (9) can be performed slot by slot. Hence, we refer to this module as slot-wise signal detection (SSD). The refined estimates of $\{y_{k,t}\}$ are forwarded to the other module. The detailed operations will be described later in Section III-B.

The module on the left hand side of Fig. 2 is for the non-linear constraints in (6). With the estimates of $\{y_{k,t}\}$ as input, the effective channels $\{g_k\}$ can be estimated based on (6). Recall that the effective channel of the same user keeps unchanged in one frame. This implies that the channel estimates for different time slots in one frame can be combined. Thus we refer to this module as combined channel estimation (CCE). With the estimates of $\{g_k\}$ improved, the estimates of $\{y_{k,t}\}$ can be updated. The output of the CCE is forwarded to the SSD module for further processing. The detailed operations of the CCE will be specified in Section III-C.

The above two modules are executed iteratively. Upon convergence, we obtain the final detection results as follows.

User identification: Let \hat{g}_k be the estimate of g_k after the last iteration. Then, a user is active if the magnitude of \hat{g}_k is larger than a certain predetermined threshold g_{th} , i.e.

$$\hat{u}_k = \begin{cases} 1 & |\hat{g}_k| \geq g_{th}, \\ 0 & |\hat{g}_k| < g_{th}. \end{cases} \quad (10)$$

Channel estimation: Let $\hat{y}_{k,t}$ be the final estimate of $y_{k,t}$, $\forall k, t$. From (6), with $\{\hat{y}_{k,t}\}$ and \hat{u}_k

available, the channel coefficient of active user k can be calculated from the reference symbol transmission (i.e., $\hat{y}_{k,1}$) as

$$\hat{h}_k = \hat{y}_{k,1}/s_p, \text{ for } \hat{u}_k = 1 \quad (11)$$

where s_p is the common reference symbol at the first column of \mathbf{X} .

Signal detection: With the estimates $\hat{y}_{k,t}$ and \hat{h}_k available, a soft estimate of the transmit signal $x_{k,t}$ (with $\hat{u}_k = 1$ and $2 \leq t \leq T$) is given by

$$\hat{x}_{k,t} = \hat{y}_{k,t}/\hat{h}_k. \quad (12)$$

Then a hard decision on $\hat{x}_{k,t}$ can be made accordingly.

B. SSD Operation

The SSD module is to estimate $\{y_{k,t}\}$ based on the received signal model (9) and the messages of $\{y_{k,t}\}$ from the CCE module. Approximate message passing type algorithms can be used to provide a near-optimal estimation of $\{y_{k,t}\}$. Specifically, we follow the GAMP algorithm [20] to leverage its low complexity and asymptotic optimality. The messages passed between the nodes are approximated by Gaussian distributions, so that only the means and variances of the messages are involved in message exchanges. In addition, instead of calculating the messages on each edge, the GAMP algorithm calculates the messages on each node [20], [24]; hence, the number of messages calculated in the algorithm is significantly reduced.

We next outline the SSD operation in each time slot t by following the GAMP algorithms [20], [21]. The detailed derivations are omitted for brevity.

1) *Initialization:* Denote by $\{m_{cxy_{k,t} \rightarrow y_{k,t}}(y_{k,t})\}$ the messages of $\{y_{k,t}\}$ fed back from CCE. (Specifically, these messages are passed from the check nodes $\{cxy_{k,t}\}$ of CCE as detailed in Section III-C.) With no feedback from CCE at the beginning, each $m_{cxy_{k,t} \rightarrow y_{k,t}}(y_{k,t})$ is initialized to $p_{y_{k,t}}(y_{k,t})$ in (8). The means $\{\hat{y}_{k,t}\}$ and variances $\{v_{y_{k,t}}\}$ of $\{y_{k,t}\}$ are calculated at variable nodes $\{y_{k,t}\}$.

2) *Message update at check nodes $\{cyr_{l,t}\}$:* Based on the linear model $z_{l,t} = \sum_{k=1}^K a_{l,k}y_{k,t}$, the messages of $\{y_{k,t}\}$ are cumulated to obtain an estimate of $\{z_{l,t}\}$. With the ‘‘Onsager’’ correction applied, the messages of $\{z_{l,t}\}$ in the form of means $\{\hat{p}_{l,t}\}$ and variances $\{v_{p_{l,t}}\}$ can be calculated as [20]

$$v_{p_{l,t}} = \sum_{k=1}^K |a_{l,k}|^2 v_{y_{k,t}}, \quad \forall l, \quad (13)$$

$$\hat{p}_{l,t} = \sum_{k=1}^K a_{l,k} \hat{y}_{k,t} - v_{p_{l,t}} \hat{s}_{l,t}, \quad \forall l, \quad (14)$$

where initially we set $\hat{s}_{l,t} = 0$ for $\forall l$. Then, the means $\{\hat{z}_{l,t}\}$ and the variances $\{v_{z_{l,t}}\}$ are computed by using the observations $\{r_{l,t}\}$ as

$$v_{z_{l,t}} = \text{Var}\{z_{l,t} | \hat{p}_{l,t}, v_{p_{l,t}}, r_{l,t}\}, \quad \forall l, \quad (15)$$

$$\hat{z}_{l,t} = \text{E}\{z_{l,t} | \hat{p}_{l,t}, v_{p_{l,t}}, r_{l,t}\}, \quad \forall l, \quad (16)$$

where the mean $\text{E}\{\cdot\}$ and variance $\text{Var}\{\cdot\}$ operations are taken with respect to the *a-posteriori* distribution of $z_{l,t}$ given the *a-priori* distribution $z_{l,t} \sim \mathcal{CN}(\hat{p}_{l,t}, v_{p_{l,t}})$ and the observation $r_{l,t} = z_{l,t} + w_{l,t}$ with $w_{l,t}$ being the l -th entry of \mathbf{w}_t . Lastly, the residual $\{\hat{s}_{l,t}\}$ and the inverse-residual-variances $\{v_{s_{l,t}}\}$ are computed by

$$v_{s_{l,t}} = (1 - v_{z_{l,t}}/v_{p_{l,t}}) / v_{p_{l,t}} \quad \forall l, \quad (17)$$

$$\hat{s}_{l,t} = (\hat{z}_{l,t} - \hat{p}_{l,t}) / v_{p_{l,t}} \quad \forall l. \quad (18)$$

3) *Message update at variable nodes $\{y_{k,t}\}$* : With the residual $\{\hat{s}_{l,t}\}$ and inverse-residual-variances $\{v_{s_{l,t}}\}$, the messages of $\{y_{k,t}\}$ are computed in the form of means $\{\hat{r}_{k,t}\}$ and variances $\{v_{r_{k,t}}\}$ as

$$v_{r_{k,t}} = \left(\sum_{l=1}^L |a_{l,k}|^2 v_{s_{l,t}} \right)^{-1}, \quad \forall k, \quad (19)$$

$$\hat{r}_{k,t} = \hat{y}_{k,t} + v_{r_{k,t}} \sum_{l=1}^L a_{l,k} \hat{s}_{l,t}, \quad \forall k. \quad (20)$$

Then the means and variances of $\{y_{k,t}\}$ are updated by

$$v_{y_{k,t}} = \text{Var}\{y_{k,t} | m_{cxy_{k,t} \rightarrow y_{k,t}}(y_{k,t}), \hat{r}_{k,t}, v_{r_{k,t}}\}, \quad \forall k, \quad (21)$$

$$\hat{y}_{k,t} = \text{E}\{y_{k,t} | m_{cxy_{k,t} \rightarrow y_{k,t}}(y_{k,t}), \hat{r}_{k,t}, v_{r_{k,t}}\}, \quad \forall k, \quad (22)$$

where the mean $\text{E}\{\cdot\}$ and variance $\text{Var}\{\cdot\}$ operations are taken with respect to the *a-posteriori* distribution of $y_{k,t}$ given its *a-priori* distribution $m_{cxy_{k,t} \rightarrow y_{k,t}}(y_{k,t})$ and the feedback message $y_{k,t} \sim \mathcal{CN}(\hat{r}_{k,t}, v_{r_{k,t}})$. These refined messages are used to update the messages of $\{z_{l,t}\}$ in the next iteration. The iteration continues until convergence or the maximum iteration number Q is reached. Finally, the messages of $\{y_{k,t}\}$ with mean $\{\hat{r}_{k,t}\}$ and variance $\{v_{r_{k,t}}\}$ are passed to the CCE module.

C. CCE Operation

With the messages $\{\hat{r}_{k,t}\}$ and $\{v_{r_{k,t}}\}$ from the SSD as input, the CCE module in Fig. 2 deals with the non-linear constraints in (6) to yield more accurate estimates of $\{y_{k,t}\}$. Since the constraints in (6) are decoupled for different users, we next present the message passing operations for each individual user as follows.

1) *Messages passed from $\{cxy_{k,t}\}$ to $\{g_k\}$* : With the output of SSD, the message from $y_{k,t}$ to $cxy_{k,t}$ is given by a complex Gaussian distribution with mean $\hat{r}_{k,t}$ and variance $v_{r_{k,t}}$, i.e., $m_{y_{k,t} \rightarrow cxy_{k,t}}(y_{k,t}) = \mathcal{CN}(\hat{r}_{k,t}, v_{r_{k,t}})$. Then, from the sum-product rule, we obtain

$$\begin{aligned} m_{cxy_{k,t} \rightarrow g_k}(g_k) &= \int_{y_{k,t}, x_{k,t}} m_{y_{k,t} \rightarrow cxy_{k,t}}(y_{k,t}) p_S(x_{k,t}) \delta(y_{k,t} - g_k x_{k,t}) \\ &= \sum_{j=1}^{|S|} \frac{p_S(s_j)}{\pi v_{r_{k,t}} / \|s_j\|^2} \exp\left(-\frac{\|g_k - \hat{r}_{k,t}/s_j\|^2}{v_{r_{k,t}} / \|s_j\|^2}\right), \quad \forall t, \end{aligned} \quad (23)$$

where $p_S(x_{k,t}) = \frac{1}{|S|} \sum_{j=1}^{|S|} \delta(x_{k,t} - s_j)$ is the *a-priori* distribution of the transmit signal $x_{k,t}$.

In (23), the algorithm assumes that the reference signals (i.e., $\{x_{k,t}\}$ with $t = 1$) are unknown and have the same *a-priori* distribution as the data. This ensures the rotational invariance of message $m_{cxy_{k,t} \rightarrow g_k}(g_k)$, i.e., $m_{cxy_{k,t} \rightarrow g_k}(g_k) = m_{cxy_{k,t} \rightarrow g_k}(g_k e^{j\theta})$, $\forall \theta \in \Omega_S$. This property is useful in developing the low-complexity algorithm in Section IV and performing state evolution analysis in Section V.

2) *Messages passed from $\{g_k\}$ to $\{cxy_{k,t}\}$* : For the same channel coefficient g_k , we have T messages $m_{cxy_{k,t} \rightarrow g_k}(g_k)$, $t = 1, \dots, T$. From the sum-product rule, we obtain

$$\begin{aligned} m_{g_k, t}(g_k) &= \prod_{t'=1, t' \neq t}^T m_{cxy_{k,t'} \rightarrow g_k}(g_k) \\ &= \prod_{t'=1, t' \neq t}^T \sum_{j=1}^{|S|} \frac{p_S(s_j)}{\pi v_{r_{k,t'}} / \|s_j\|^2} \exp\left(-\frac{\|g_k - \hat{r}_{k,t'}/s_j\|^2}{v_{r_{k,t'}} / \|s_j\|^2}\right), \quad \forall t, \end{aligned} \quad (24)$$

$$m_{g_k \rightarrow cxy_{k,t}}(g_k) = m_{g_k, t}(g_k) p_{G_k}(g_k), \quad \forall t, \quad (25)$$

where $p_{G_k}(g_k)$ is the *a-priori* distribution of the effective channel g_k given in (7).

3) *Messages passed from $\{cxy_{k,t}\}$ to $\{y_{k,t}\}$* : With the message $m_{g_k \rightarrow cxy_{k,t}}(g_k)$ from node g_k , we obtain

$$\begin{aligned} m_{cxy_{k,t} \rightarrow y_{k,t}}(y_{k,t}) &= \int_{g_k, x_{k,t}} m_{g_k \rightarrow cxy_{k,t}}(g_k) p_S(x_{k,t}) \delta(y_{k,t} - g_k x_{k,t}) \\ &= \sum_{j=1}^{|S|} p_S(s_j) m_{g_k \rightarrow cxy_{k,t}}(y_{k,t}/s_j), \quad \forall t. \end{aligned} \quad (26)$$

These messages are passed to the variable nodes $\{y_{k,t}\}$ to activate the next SSD operation. The

SSD and CCE operations iterate until convergence.

D. Overall Algorithm and Complexity Analysis

Based on the procedures described in Section III-B and Section III-C, we outline the main steps of the proposed JUICESD algorithm in Algorithm 1, where Q is the maximum number of iterations allowed in the SSD module, and Q' is the maximum number of iterations between the SSD and CCE modules.

Algorithm 1 JUICESD Algorithm

Input: Received signal \mathbf{R} , signature matrix \mathbf{A} , signal distribution $p_S(s)$, channel distributions $\{p_{H_k}(\cdot)\}$, user activity probability λ .

for $q' = 1, 2, \dots, Q'$

$\backslash \backslash$ SSD module

Initialization: $\hat{y}_{k,t} = E\{y_{k,t}\}$, $v_{y_{k,t}} = \text{Var}\{y_{k,t}\}$, $\hat{s}_{l,t}^{(0)} = 0$;

for $q = 1, 2, \dots, Q$

 Calculate $v_{z_{l,t}}$ and $\hat{z}_{l,t}$, $\forall l, t$, based on (13)-(16);

 Calculate $v_{y_{k,t}}$ and $\hat{y}_{k,t}$, $\forall k, t$, based on (17)-(22);

end

$\backslash \backslash$ CCE module

 Calculate the message of g_k in each time slot using (23);

 Calculate the message of g_k by combining multiple messages in multiple time slots and the *a-priori* distribution of g_k using (24) and (25);

 Calculate the refined messages of $\{y_{k,t}\}$ using (26);

end

Output: Obtain the final estimates $\{\hat{u}_k\}$, $\{\hat{h}_k\}$ and $\{\hat{x}_{k,t}\}$ according to (10)-(12).

The complexity of the JUICESD algorithm is described as follows. The algorithm consists of two modules: SSD and CCE. The SSD operation is based on slot-wise GAMP; hence, its complexity is $\mathcal{O}(KLT)$. The complexity of the CCE operation is dominated by (24). Recall that (24) is the product of $(T - 1)$ $|\mathcal{S}|$ -component Gaussian mixtures. A direct evaluation of (24) results in a complexity of $\mathcal{O}(KT|\mathcal{S}|^{T-1})$ for the CCE. Consequently, the total complexity of JUICESD is $\mathcal{O}(KLT + KT|\mathcal{S}|^{T-1})$. This complexity is linear in the number of users and the spreading length, but exponential with respect to the frame length T . Clearly, the proposed JUICESD algorithm is well suited for the case of massive connections with very short packets. For mMTC scenarios with medium-size or relatively long packets, its complexity could become unaffordable in practice. To address this issue, we further propose the JUICESD-RiGm algorithm as detailed in Section IV.

Algorithm 1 assumes that the reference signals are unknown during the iteration; see (23) and the discussions therein. Yet, the knowledge of the reference signals $\{x_{k,1}, \forall k\}$ are used only in the final step to remove the phase ambiguity of the output. Alternatively, we may incorporate the knowledge of the reference signals into the iterative process by letting $p_S(x_{k,1}) = \delta(x_{k,1} - s_p)$, $\forall k$, in (23). Numerical results show that these two approaches in fact result in almost the same performance. However, an disadvantage for the latter approach is that the rotational invariance property of messages no longer holds in (23) and (24). This would prevent further development of the low-complexity yet efficient algorithm as the rotational invariance property plays an essential role in establishing the next JUICESD-RiGm algorithm and its state evolution analysis.

IV. JUICESD-RiGM ALGORITHM

Given that the modulation constellation \mathcal{S} has an rotational invariance property with respect to the angle set Ω_S , we can introduce a rotationally invariant Gaussian mixture (RiGm) model to alleviate the complexity burden of the JUICESD algorithm.

A. Preliminaries

Recall that (24) is the product of $(T - 1)$ $|\mathcal{S}|$ -component Gaussian mixtures. There are $|\mathcal{S}|^{T-1}$ Gaussian components in (24) in general, and a direct evaluation of (24) can be very complicated especially for a medium or large T . The complexity can be reduced to be linear in T if we discretize each $|\mathcal{S}|$ -component Gaussian mixture by sampling and then evaluate (24) approximately based on the discrete samples. However, due to the high dynamic range of the means and variances involved in (24), the complexity of this sampling approach is still high since a large number of samples are required to ensure a good approximation of (24).

Another approach is to rely on the Gaussian approximation that is widely used in the design of approximate message passing algorithms [33], [34], [37]. However, simply approximating (24) by a Gaussian distribution can lead to a substantial information loss and consequently incurs evident performance degradation, as demonstrated by the numerical results in Section VI.¹ The reason for this performance degradation is possibly the phase ambiguity aforementioned for problem (4). Due to the phase ambiguity, there are usually multiple Gaussian components with equal

¹For Gaussian approximation, the knowledge of the reference signals should be utilized in the iterative process of the algorithm, i.e., the *a-priori* of each $x_{k,1}$ should be set to $p_S(x_{k,1}) = \delta(x_{k,1} - s_p)$, $\forall k$. Otherwise, the algorithm with Gaussian approximation fails by noting that the means of the messages in (23) and (24) are always zeros due to the rotational invariance property.

importance in (24), while the number of equally important Gaussian components is determined by the geometric symmetry of the modulation constellation. This inspires us to use a RiGm model for message approximation, as described next.

B. Rotationally Invariant Gaussian Mixture Approximation

Recall that due to the phase ambiguity, if \hat{g}_k is an estimate of the effective channel of user k , then $e^{j\theta}\hat{g}_k, \forall \theta \in \Omega_S \equiv \{\theta_0, 2\theta_0, \dots, |\Omega_S|\theta_0\}$ is also a valid estimate of the channel as *good* as \hat{g}_k . For this reason, we approximate the $|\mathcal{S}|^{T-1}$ -component Gaussian mixture in (24) by a $|\Omega_S|$ -component Gaussian mixture (GM) with the following form:

$$m_{g_k,t}(g_k) = \sum_{i=1}^{|\Omega_S|} \frac{1}{|\Omega_S| \pi v_{g_k,t}} \exp\left(-\frac{\|g_k - \hat{g}_{k,t,i}\|^2}{v_{g_k,t}}\right), \quad (27)$$

where $\hat{g}_{k,t,i}$ is the mean of the i -th Gaussian component satisfying $\hat{g}_{k,t,i} = e^{j(i-1)\theta_0}\hat{g}_{k,t,1}$, and $v_{g_k,t}$ is the common variance for all the Gaussian components. We note that the GM in (27) is rotationally invariant over the angle set Ω_S . Hence we refer to it as rotationally invariant GM (RiGm). The rotational invariance property of RiGm enables the characterization of (27) by only two parameters, namely, the component mean $\hat{g}_{k,t,i}$ and the variance $v_{g_k,t}$. This simplifies the message calculation, and also facilitates the development of the state evolution analysis in Section V.

We next describe how to calculate the parameters $\{\hat{g}_{k,t,i}\}$ and $\{v_{g_k,t}\}$ in (27). Without loss of generality, we focus on the case of $t = 1$, where $m_{g_k,t}(g_k)$ in (24) is given by

$$m_{g_k,1}(g_k) = \prod_{t'=2}^T m_{cxy_{k,t'} \rightarrow g_k}(g_k) = \prod_{t'=2}^T \sum_{j=1}^{|\mathcal{S}|} \frac{p_{\mathcal{S}}(s_j)}{\pi v_{r_{k,t'}} / \|s_j\|^2} \exp\left(-\frac{\|g_k - \hat{r}_{k,t'} / s_j\|^2}{v_{r_{k,t'}} / \|s_j\|^2}\right). \quad (28)$$

We adopt a recursive method as follows. Assume that the first $T' - 1$ factors in the product in (28) have been approximated by a $|\Omega_S|$ -component RiGm, denoted by $m_{g_k,1}^{(T')}(g_k)$. We then approximate the product of $m_{g_k,1}^{(T')}(g_k)$ and $m_{cxy_{k,T'+1} \rightarrow g_k}(g_k)$ by a $|\Omega_S|$ -component RiGm, denoted by $m_{g_k,1}^{(T'+1)}(g_k)$. This process continues until $m_{g_k,1}^{(T)}(g_k)$ is obtained, which gives the approximation of (28) in the form of (27). Below we present the details involved in the recursive method.

1) *Initialization*: We need to approximate $m_{cxy_{k,2} \rightarrow g_k}(g_k)$ by a $|\Omega_S|$ -component RiGm. Recall that \mathcal{S} is rotationally invariant with respect to $\Omega_S = \{\theta_0, 2\theta_0, \dots, |\Omega_S|\theta_0\}$. We divide \mathcal{S} into $|\Omega_S|$ subsets, each with $|\mathcal{S}|/|\Omega_S|$ elements. Each subset i contains the constellation points with

the phase angles falling into the range of $[(i-1)\theta_0, i\theta_0]$, for $i = 1, \dots, |\Omega_S|$. We denote the i -th subset as

$$\mathcal{S}_i \doteq \{s_{i,1}, s_{i,2}, \dots, s_{i,|\mathcal{S}|/|\Omega_S|}\}, \quad i = 1, 2, \dots, |\Omega_S|. \quad (29)$$

It can be verified that $\{\mathcal{S}_i\}$ is a partition of \mathcal{S} , and $\mathcal{S}_i = e^{j(i-1)\theta_0} \mathcal{S}_1$.

Using (29), we rewrite $m_{\text{cxy}_{k,2} \rightarrow g_k}(g_k)$ in (28) (i.e., the multiplicative component for $t' = 2$) as

$$\sum_{i=1}^{|\Omega_S|} \sum_{m=1}^{|\mathcal{S}|/|\Omega_S|} \frac{1}{|\mathcal{S}| \pi v_{r_{k,2}} / \|s_{i,m}\|^2} \exp \left(-\frac{\|g_k - \hat{r}_{k,2}/s_{i,m}\|^2}{v_{r_{k,2}} / \|s_{i,m}\|^2} \right). \quad (30)$$

We then approximate the $|\mathcal{S}|/|\Omega_S|$ Gaussian components in (30) related to subset \mathcal{S}_i by a single Gaussian component and obtain the $|\Omega_S|$ -component GM approximation of (30) as

$$\sum_{i=1}^{|\Omega_S|} \frac{1}{|\Omega_S| \pi v_{g_k,i}^{(2)}} \exp \left(-\frac{\|g_k - \hat{g}_{k,i}^{(2)}\|^2}{v_{g_k,i}^{(2)}} \right), \quad (31)$$

where

$$\hat{g}_{k,i}^{(2)} = \frac{1}{|\mathcal{S}|/|\Omega_S|} \sum_{m=1}^{|\mathcal{S}|/|\Omega_S|} \frac{\hat{r}_{k,2}}{s_{i,m}}, \quad (32a)$$

$$v_{g_k,i}^{(2)} = \frac{1}{|\mathcal{S}|/|\Omega_S|} \sum_{m=1}^{|\mathcal{S}|/|\Omega_S|} \left(\frac{v_{r_{k,2}}}{\|s_{i,m}\|^2} + \left\| \frac{\hat{r}_{k,2}}{s_{i,m}} \right\|^2 \right) - \|\hat{g}_{k,i}^{(2)}\|^2. \quad (32b)$$

With $\mathcal{S}_i = e^{j(i-1)\theta_0} \mathcal{S}_1$, we can verify in (31) that: 1) $\hat{g}_{k,i}^{(2)} = e^{j(i-1)\theta_0} \hat{g}_{k,1}^{(2)}, \forall i$, and 2) $\{v_{g_k,i}^{(2)}, \forall i\}$ share a common value denoted by $v_{g_k}^{(2)}$. Hence, (31) satisfies the RiGM requirement. Fig. 3(a) shows an example of such an approximation process for the 16QAM constellation, where $\mathcal{S} = 16$, $|\Omega_S| = 4$, and $\theta_0 = 0.5\pi$.

2) *Recursion*: We need to approximate the product of $m_{g_k,1}^{(T')}(g_k)$ and $m_{\text{cxy}_{k,T'+1} \rightarrow g_k}(g_k)$ by a $|\Omega_S|$ -component RiGm. To this end, we multiply each Gaussian component in $m_{g_k,1}^{(T')}(g_k)$ with $m_{\text{cxy}_{k,T'+1} \rightarrow g_k}(g_k)$, and then approximate the result by a new Gaussian component, as illustrated in Fig. 3(b).

Suppose that $m_{g_k,1}^{(T')}(g_k)$ is given by

$$m_{g_k,1}^{(T')}(g_k) = \sum_{i=1}^{|\Omega_S|} \frac{1}{|\Omega_S| \pi v_{g_k}^{(T')}} \exp \left(-\frac{\|g_k - \hat{g}_{k,i}^{(T')}\|^2}{v_{g_k}^{(T')}} \right), \quad \text{for } T' = 2, \dots, T-1, \quad (33)$$

where $\hat{g}_{k,i}^{(T')}$ is the mean of the i -th Gaussian component satisfying $\hat{g}_{k,i}^{(T')} = e^{j(i-1)\theta_0} \hat{g}_{k,1}^{(T')}$, and $v_{g_k}^{(T')}$ is the common variance for all the Gaussian components. For $T' = 2$, (33) is initialized by (31).

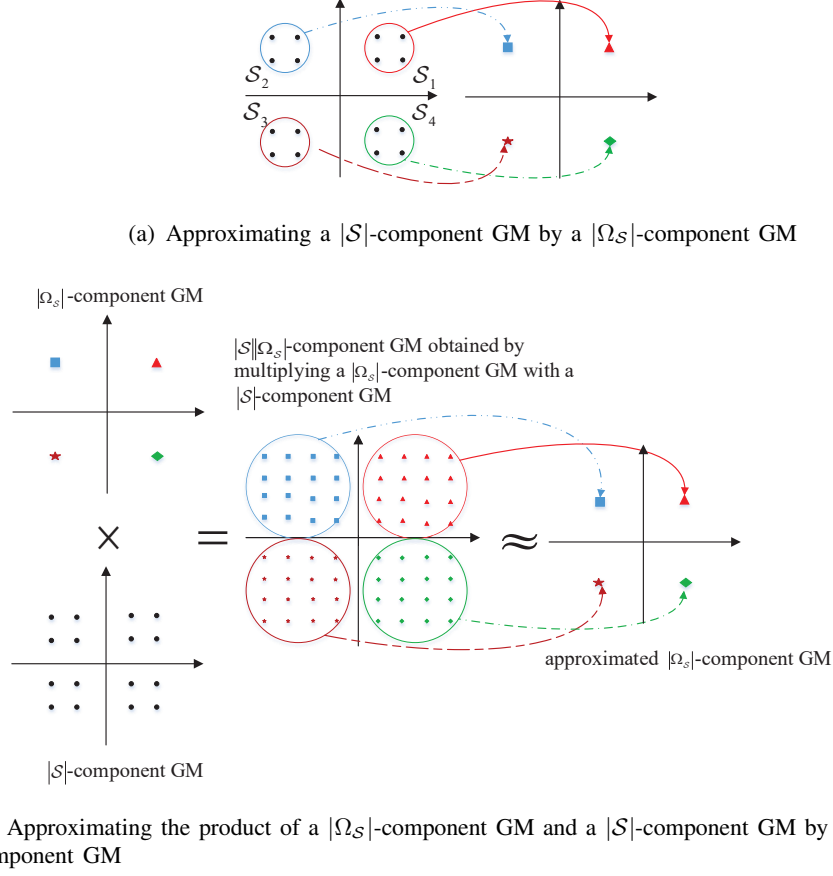


Fig. 3. An illustration of the basic operations in approximating (24) by (27).

The product of $m_{cxy_{k,T'+1} \rightarrow g_k}(g_k)$ and the i -th Gaussian component of $m_{g_k,1}^{(T')}(g_k)$ is still a GM, expressed by $\sum_{j=1}^{|\mathcal{S}|} w_{i,j}^{(T')} \mathcal{CN}(\mu_{i,j}^{(T')}, \tau_{i,j}^{(T')})$, where

$$w_{i,j}^{(T')} \propto \frac{1}{\pi(v_{g_k}^{(T')} + v_{r_{k,T'+1}}/\|s_j\|^2)} \exp\left(-\frac{\|\hat{g}_{k,i}^{(T')} - \hat{r}_{k,T'+1}/s_j\|^2}{v_{g_k}^{(T')} + v_{r_{k,T'+1}}/\|s_j\|^2}\right) \text{ with } \sum_{j=1}^{|\mathcal{S}|} w_{i,j}^{(T')} = 1, \quad (34a)$$

$$\mu_{i,j}^{(T')} = \frac{\hat{g}_{k,i}^{(T')} v_{r_{k,T'+1}}/\|s_j\|^2 + v_{g_k}^{(T')} \hat{r}_{k,T'+1}/s_j}{v_{g_k}^{(T')} + v_{r_{k,T'+1}}/\|s_j\|^2} \text{ and } \tau_{i,j}^{(T')} = \frac{v_{g_k}^{(T')} v_{r_{k,T'+1}}/\|s_j\|^2}{v_{g_k}^{(T')} + v_{r_{k,T'+1}}/\|s_j\|^2}. \quad (34b)$$

By using moment matching principle, we approximate this GM by a new Gaussian distribution $\mathcal{CN}(\hat{g}_{k,i}^{(T'+1)}, v_{g_k,i}^{(T'+1)})$ with

$$\hat{g}_{k,i}^{(T'+1)} = \sum_{j=1}^{|\mathcal{S}|} w_{i,j}^{(T')} \mu_{i,j}^{(T')} \text{ and } v_{g_k,i}^{(T'+1)} = \sum_{j=1}^{|\mathcal{S}|} w_{i,j}^{(T')} \left(\tau_{i,j}^{(T')} + \|\mu_{i,j}^{(T')}\|^2 \right) - \|\hat{g}_{k,i}^{(T'+1)}\|^2. \quad (35)$$

Performing the same operation for the other $|\Omega_{\mathcal{S}}| - 1$ components in $m_{g_k,1}^{(T')}(g_k)$, we obtain a $|\Omega_{\mathcal{S}}|$ -component GM

$$m_{g_k,1}^{(T'+1)}(g_k) = \sum_{i=1}^{|\Omega_S|} \frac{1}{|\Omega_S| \pi v_{g_k}^{(T'+1)}} \exp \left(-\frac{\|g_k - \hat{g}_{k,i}^{(T'+1)}\|^2}{v_{g_k}^{(T'+1)}} \right). \quad (36)$$

The rotational invariance property of (36) is ensured by the following lemma.

Lemma 1: The message in (36) is rotationally invariant over the angle set Ω_S , i.e.,

$$\hat{g}_{k,i}^{(T'+1)} = e^{j(i-1)\theta_0} \hat{g}_{k,1}^{(T'+1)}, \quad \forall i, \quad (37a)$$

$$v_{g_k,1}^{(T'+1)} = v_{g_k,2}^{(T'+1)} = \dots = v_{g_k,|\Omega_S|}^{(T'+1)} \equiv v_{g_k}^{(T'+1)}, \quad \text{for } T' = 2, \dots, T-1. \quad (37b)$$

Proof: See Appendix A.

C. CCE Based on RiGm Approximation

With the replacement of (24) by (27), we can rewrite (26) as

$$m_{cxy_{k,t} \rightarrow y_{k,t}}(y_{k,t}) = w_{k,t} \delta(y_{k,t}) + \sum_{j=1}^{|\mathcal{S}|} \frac{1 - w_{k,t}}{|\mathcal{S}| \pi v_{y_{k,t},j}} \exp \left(-\frac{\|y_{k,t} - \hat{y}_{k,t,j}\|^2}{v_{y_{k,t},j}} \right) \quad (38)$$

where the weight of the impulse term is given by

$$w_{k,t} = \frac{\sum_{i=1}^{|\Omega_S|} \frac{1-\lambda}{|\Omega_S| \pi v_{g_k,t}} \exp \left(-\frac{\|\hat{g}_{k,t,i}\|^2}{v_{g_k,t}} \right)}{\sum_{i=1}^{|\Omega_S|} \left(\frac{1-\lambda}{|\Omega_S| \pi v_{g_k,t}} \exp \left(-\frac{\|\hat{g}_{k,t,i}\|^2}{v_{g_k,t}} \right) + \frac{\lambda}{|\Omega_S| \pi (v_{g_k,t} + \beta_k)} \exp \left(-\frac{\|\hat{g}_{k,t,i}\|^2}{v_{g_k,t} + \beta_k} \right) \right)} \quad (39a)$$

and the variance and the mean of the j -th Gaussian component are respectively

$$v_{y_{k,t},j} = \frac{\beta_k v_{g_k,t} \|s_j\|^2}{\beta_k + v_{g_k,t}} \quad \text{and} \quad \hat{y}_{k,t,j} = \frac{\hat{g}_{k,t,1} \beta_k s_j}{\beta_k + v_{g_k,t}} \quad (39b)$$

Finally, the JUICESD-RiGm algorithm is obtained by replacing (24) and (26) in the JUICESD algorithm with (27) and (38), respectively.

D. Overall Algorithm

The proposed JUICESD-RiGm algorithm is outlined in Algorithm 2. Based on the rotational invariance property in Lemma 1, the complexity of evaluating (27) in the CCE operation is $\mathcal{O}(|\mathcal{S}|T)$ (with the complexities of computing (31) and (35) given by $\mathcal{O}(|\mathcal{S}|/|\Omega_S|)$ and $\mathcal{O}(|\mathcal{S}|)$, respectively). Following the arguments in the JUICESD case, we see that the total complexity of the proposed JUICESD-RiGm algorithm becomes $\mathcal{O}(KLT + KT^2|\mathcal{S}|)$. This complexity is clearly much lower than that of the original JUICESD algorithm, especially for relatively large T . This implies that the proposed JUICESD-RiGm algorithm can provide an attractive solution for massive connection scenarios with both short and relatively long packets.

Algorithm 2 JUICESD-RiGm Algorithm

Input: Received signal \mathbf{R} , signature matrix \mathbf{A} , signal distribution $p_S(s)$, channel distributions $\{p_{H_k}(\cdot)\}$, user activity probability λ .

for $q' = 1, 2, \dots, Q'$

 \\ SSD module

Initialization: $\hat{y}_{k,t} = E\{y_{k,t}\}$, $v_{y_{k,t}} = \text{Var}\{y_{k,t}\}$, $\hat{s}_{l,t}^{(0)} = 0$;

for $q = 1, 2, \dots, Q$

 Calculate $v_{z_{l,t}}$ and $\hat{z}_{l,t}$, $\forall l, t$, based on (13)-(16);

 Calculate $v_{y_{k,t}}$ and $\hat{y}_{k,t}$, $\forall k, t$, based on (17)-(22);

end

 \\ CCE module

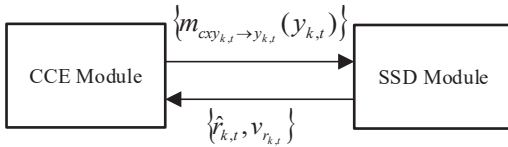
 Calculate the message of g_k in each time slot according to (23);

 Calculate the message of g_k by combining multiple messages in multiple time slots and the *a-priori* distribution of g_k according to (27) and (25);

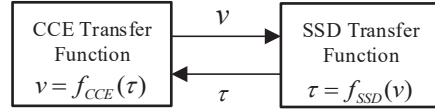
 Calculate the refined messages of $\{y_{k,t}\}$ according to (38);

end

Output: Obtain the final estimates $\{\hat{u}_k\}$, $\{\hat{h}_k\}$ and $\{\hat{x}_{k,t}\}$ according to (10)-(12).



(a) Structure of the proposed iterative algorithm



(b) The corresponding state evolution

Fig. 4. Structure of the proposed iterative algorithm and the corresponding state evolution

V. STATE EVOLUTION OF JUICESD-RiGM

We now describe the state evolution of the JUICESD-RiGm algorithm. Recall that in JUICESD-RiGm, we divide the whole receiver into two modules, i.e., the SSD module and the CCE module as shown in Fig. 4(a). Our approach is to characterize the behavior of each module by tracking their input and output mean-square errors (MSEs).

More specifically, as illustrated in Fig. 4(b), we aim to characterize the behavior of the SSD module by the transfer function $\tau = f_{SSD}(v)$ where v and τ are the input and output MSEs of the SSD module, respectively. Correspondingly, the CCE module can be characterized by the transfer function $v = f_{CCE}(\tau)$ where τ and v are the input and output MSEs of the CCE module, respectively. Then, the performance of the JUICESD-RiGm algorithm is determined by the fixed point of

$$v = f_{CCE}(f_{SSD}(v)). \quad (40)$$

A. SSD Transfer Function

Consider the establishment of the SSD transfer function $\tau = f_{SSD}(v)$. It is desirable to directly express the generation model of the input messages of the SSD module in (38) by the single parameter v . Unfortunately, this is difficult since (38) is determined by three sets of variables $\{w_{k,t}\}$, $\{\hat{y}_{k,t,j}\}$, and $\{v_{y_{k,t,j}}\}$. Instead of directly generating the messages in (38), we notice that the messages in (38) are actually determined by the messages in (27). We can model the messages in (27) using a single parameter v_g . Specifically, we model each $\hat{g}_{k,t}$ by

$$\hat{g}_{k,t} = g_k + \sqrt{v_g} \zeta_{k,t} \quad (41)$$

where $g_k \sim f_{G_k}(g_k)$, and each $\zeta_{k,t}$ is independently drawn from $\mathcal{CN}(0, 1)$. Then, from the rotational invariance property, the whole set $\{\hat{g}_{k,t,i}\}$ is given by $\{e^{-j\theta_i} \hat{g}_{k,t}, \theta_i \in \Omega_S, i = 1, \dots, |\Omega_S|\}$. We next show how to determine v_g for a given v . Recall that $\{v_{y_{k,t,j}}, j = 1, \dots, |\mathcal{S}|\}$ in (38) are the variances with respect to different component Gaussian distributions. We define the input MSE v to the SSD module as

$$v = \frac{1}{KT|\mathcal{S}|} \sum_{k,t,j} v_{y_{k,t,j}}. \quad (42)$$

Substituting the first equation of (39b) into (42) and letting $v_{g_{k,t}} = v_g$ for $\forall k, t$, we obtain

$$v = \frac{1}{|\mathcal{S}|K} \sum_k \frac{\beta_k v_g}{\beta_k + v_g} \sum_{j=1}^{|\mathcal{S}|} \|s_j\|^2 = \frac{1}{K} \sum_k \frac{\beta_k v_g}{\beta_k + v_g}. \quad (43)$$

Then v_g can be obtained according to the given v by solving (43).

We now summarize the generation process of the input messages. We first calculate v_g from v using (43), and then generate $\{\hat{g}_{k,t}\}$ using (41). We rotate $\hat{g}_{k,t}$ based on Ω_S to obtain $\{\hat{g}_{k,t,i}\}$ and then the messages in (27). Finally, we obtain the input messages to SSD in the form of (38). With the above input model, we construct the SSD transfer function $\tau = f_{SSD}(v)$ as follows.

Recall that the SSD module is an AMP-type algorithm. Similarly to the state evolution of the AMP algorithm [24], we derive the SSD transfer function by tracking the equivalent noise-and-interference power seen by each user. Given the input messages $\{m_{cxy_{k,t} \rightarrow y_{k,t}}(y_{k,t})\}$, let $Y_{k,t}$ be a random variable with the distribution $m_{cxy_{k,t} \rightarrow y_{k,t}}(y_{k,t})$. We initialize the equivalent noise-and-interference power seen by each user as

$$\tau^{(0)} \equiv \frac{1}{KT} \sum_{k,t} \left(N_0 + \frac{K-1}{L} E_{Y_{k,t}} \{|Y_{k,t}|^2\} \right), \quad (44)$$

where $E_{Y_{k,t}}\{|Y_{k,t}|^2\}$ is the interference power caused by $Y_{k,t}$ when there is no interference cancellation; the term $K - 1$ implies that each user suffers from the interference of $K - 1$ users; and the term $1/L$ comes from the spreading/de-spreading operations. Then we calculate $\tau^{(q)}$ recursively for $q \geq 0$ as follows. With $\tau^{(q)}$ given, each user performs the *a-posteriori* estimation to obtain a refined estimate with a reduced residual interference power. Let $E\{Y_{k,t}|Y_{k,t} + \sqrt{\tau^{(q)}}\epsilon, \tau^{(q)}\}$ be the *a-posteriori* estimate function in (22) in the SSD module, where $Y_{k,t} \sim m_{cxy_{k,t} \rightarrow y_{k,t}}(y_{k,t})$ and $\epsilon \sim \mathcal{CN}(0, 1)$. Then the residual interference power of $Y_{k,t}$ after its *a-posteriori* estimation is $E_{\{Y_{k,t}, \epsilon\}} \left(\left| E\{Y_{k,t}|Y_{k,t} + \sqrt{\tau^{(q)}}\epsilon, \tau^{(q)}\} - Y_{k,t} \right|^2 \right)$. Consequently, the equivalent noise-and-interference power seen by each user is updated by

$$\tau^{(q+1)} = \frac{1}{KT} \sum_{k,t} \left(N_0 + \frac{K-1}{L} E_{\{Y_{k,t}, \epsilon\}} \left(\left| E\{Y_{k,t}|Y_{k,t} + \sqrt{\tau^{(q)}}\epsilon, \tau^{(q)}\} - Y_{k,t} \right|^2 \right) \right), \quad (45)$$

where $Y_{k,t} \sim m_{cxy_{k,t} \rightarrow y_{k,t}}(y_{k,t})$ and $\epsilon \sim \mathcal{CN}(0, 1)$. $\tau^{(q+1)}$ in (45) is calculated recursively until convergence, and the fixed point τ gives the output MSE of the SSD. The transfer function $\tau = f_{SSD}(v)$ is then obtained.

B. CCE Transfer Function

We now describe how to determine the CCE transfer function $v = f_{CCE}(\tau)$. As analogous to the SSD case, we need to construct a generation model of the input messages $\{\hat{r}_{k,t}, v_{r_{k,t}}\}$ of the CCE by using a single parameter τ . In this regard, we model each $\hat{r}_{k,t}$ as

$$\hat{r}_{k,t} = h_k u_k x_{k,t} + \sqrt{\tau} \zeta_{k,t}, \quad \text{for } \forall k, t \quad (46)$$

where $h_k \sim p_{H_k}(h_k)$, $x_{k,t} \sim p_S(x_{k,t})$, and $\zeta_{k,t} \sim \mathcal{CN}(0, 1)$. We observe from numerical results that the output MSEs for the active users and inactive users can be quite different. Note that the user activity state u_k can be estimated by the algorithm with very high accuracy, especially for a relatively large T . And for an inactive user with known $u_k = 0$, both its channel estimation error and its symbol error rate can be regarded as zero. In this case, we will only consider the active users with $u_k = 1$ to simplify the analysis.

With the input messages $\{\hat{r}_{k,t}\}$ generated based on (46) and assuming $v_{r_{k,t}} = \tau$, $\forall k, t$, we obtain the output messages $m_{cxy_{k,t} \rightarrow y_{k,t}}(y_{k,t})$ of the CCE module by following (23), (27), and (38). Then, the output MSE v is given by the average of the output variances $v_{y_{k,t},j}$ over k, t and j . The CCE transfer function $v = f_{CCE}(\tau)$ is thus obtained.

C. Further Discussions

The state evolution of the proposed JUICESD-RiGm algorithm is given by the nested recursion in (40), and the algorithm performance can be predicted by the fixed point of (40). In practice, both $f_{SSD}(\cdot)$ and $f_{CCE}(\cdot)$ need to be pre-simulated and stored as a look-up table. We will show by numerical results that the recursion in (40) can accurately predict the algorithm performance. As a result, the state evolution technique provides a fast and effective performance analysis tool for the JUICESD-RiGm algorithm.

VI. NUMERICAL RESULTS

In this section, we provide numerical results to verify the effectiveness of the proposed algorithms. The signal-to-noise ratio (SNR) is defined by $SNR = \frac{1}{N_0}$ (for normalized signal constellation \mathcal{S} with $\sum_{j=1}^{|\mathcal{S}|} \|s_j\|^2 / |\mathcal{S}| = 1$). The data signals of all active users are QPSK modulated. In simulations, we mainly focus on the case that perfect power control is adopted to compensate for large scale fading such that $\beta_1 = \beta_2 = \dots = \beta_K \equiv 1$. We will briefly discuss the impact of large scale fading in the last subsection.

A. Error Rate Performance

We first define the activity error rate (AER) and the symbol error rate (SER) in the considered systems. For each frame, if the activities of all users are correct, the activity error is 0; otherwise, the activity error is 1. The AER is then obtained as the average of the activity errors over all simulated frames. The SER is calculated as follows. For inactive users, if its active state is judged correctly, all symbols are regarded as detected correctly; otherwise all incorrectly. For active users, we estimate their transmitted QPSK signals. A symbol is detected correctly only when both the user activity and the user symbol are judged correctly.

In Fig. 5, we compare the AER and SER performance of our proposed algorithms with the state-of-the-art BSASP algorithm in [36]. For comparison, we also include the performance of the two-phase detection scheme [30] in which the receiver first estimates the user activities and channel coefficients jointly, and then recovers the signals sent by the active users, both through AMP algorithms. In addition, we include the performance for JUICESD with message sampling in evaluating (24) (simply referred to as JUICESD) as a benchmark, and that for a so-called JUICESD-GA algorithm where the simple Gaussian approximation is used for message updates in the CCE module of the proposed JUICESD algorithm.

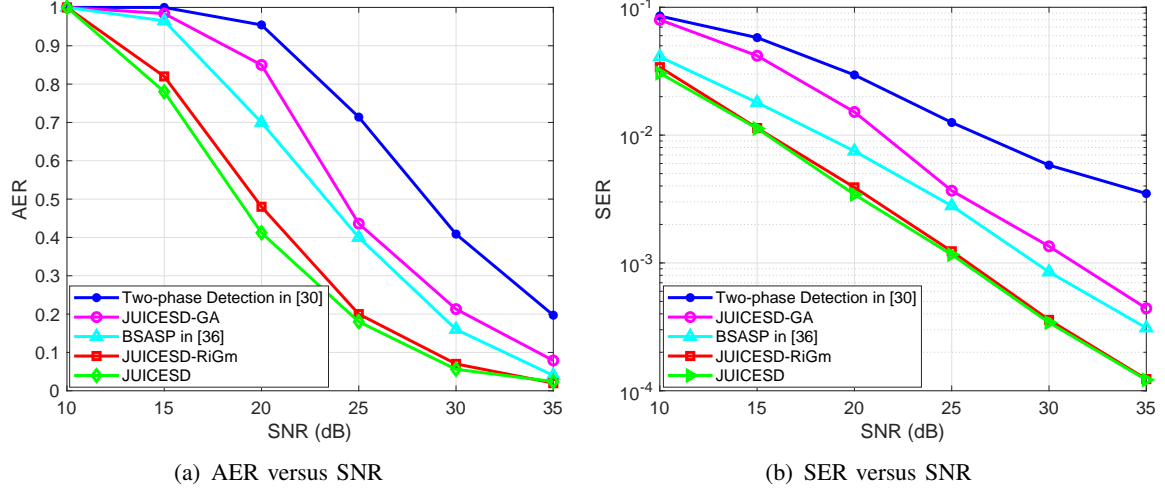


Fig. 5. Performance versus SNR: $K = 200$, $L = 50$, $\lambda = 0.1$, $T = 7$.

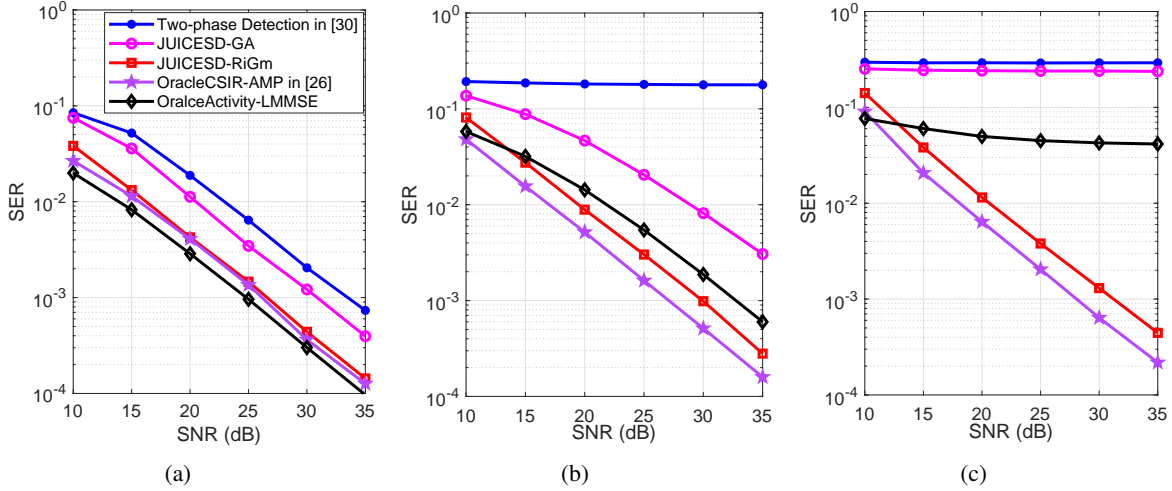


Fig. 6. SER versus SNR: $K = 2000$, $L = 500$, $T = 7$. (a) $\lambda = 0.1$, (b) $\lambda = 0.2$, and (c) $\lambda = 0.3$.

From Fig. 5, we see that the two-phase detection scheme has a relatively high error floor while the BSASP and proposed JUICESD-RiGm algorithms work well. This demonstrates the benefit of joint user identification, channel estimation, and signal detection design. Furthermore, the proposed JUICESD-RiGm algorithm outperforms BSASP by about 3 – 4 dB in terms of AER and SER. This is because BSASP suffers from non-orthogonal training, while the proposed JUICESD-RiGm algorithm relies on message passing principles to iteratively cancel/suppress the interference among users. Lastly, the JUICESD-RiGm algorithm and the (higher-complexity) JUICESD algorithm have similar performance. This implies that the proposed rotationally invariant Gaussian mixture model provides a good approximation for the complicated message

involved in the joint design. On the other hand, the JUICESD-GA has an evident performance degradation due to its over-simplified Gaussian message structure.

We next apply the two-phase detection scheme, JUICESD-GA, and JUICESD-RiGm to a much larger system. We set the number of potential users $K = 2000$, the length of spreading sequence $L = 500$. We use the OracleActivity-LMMSE (in which user activity information is assumed to be perfectly known while both channel and data are estimated based on LMMSE principles) and the OracleCSIR-AMP in [26] (in which perfect CSIR is assumed and the user activity and data are jointly detected by using AMP) as baselines. Fig. 6 shows the SER performance of the considered algorithms. It can be seen that the proposed JUICESD-RiGm algorithm always outperforms the two-phase detection scheme, and it achieves a substantial performance improvement over JUICESD-GA. In addition, JUICESD-RiGm only has a small SER gap to OracleCSIR-AMP especially when the user activity probability λ is small. This implies that JUICESD-RiGm can estimate the channel accurately through joint detection. Note that JUICESD-RiGm outperforms OracleActivity-LMMSE when λ is large (i.e., $\lambda = 0.2, 0.3$). This is possible since LMMSE is a linear detection algorithm that strictly sub-optimal when a finite constellation alphabet is employed in modulation.

B. Phase Transition Performance

Fig. 7 shows the phase transition performance of the proposed JUICESD-RiGm algorithm, where λ is the user active probability and $\gamma = L/K$. A transmission is declared as a success if its SER is lower than a given threshold SER_{th} ; otherwise the transmission is declared as a failure. The phase transition curve in Fig. 7 divides the whole region into the upper-left success region and the lower-right failure region. It is observed from Fig. 7 that the system load supported by JUICESD-RiGm is much larger than the other two baseline algorithms. For example, at $\gamma = L/K = 0.1$, JUICESD-RiGm can support activity probability of $\lambda = 0.13$, which is much greater than $\lambda = 0.05$ for JUICESD-GA and $\lambda = 0.03$ for the two-phase detection scheme. It can be seen in the phase transition that the JUICESD-RiGm algorithm can achieve a good performance even when $\lambda > \gamma$, and closely approaches the OracleCSIR-AMP curve throughout the considered range of λ . Note that $\lambda > \gamma$ implies the number of active users supported by the system exceeds the spreading length L . This is possible because the user activities are fixed across T slots (effectively increasing the number of observations by a factor of $T = 7, 14$) and because of non-ideal coding (i.e., QPSK with $SER_{th} = 10^{-3}$).

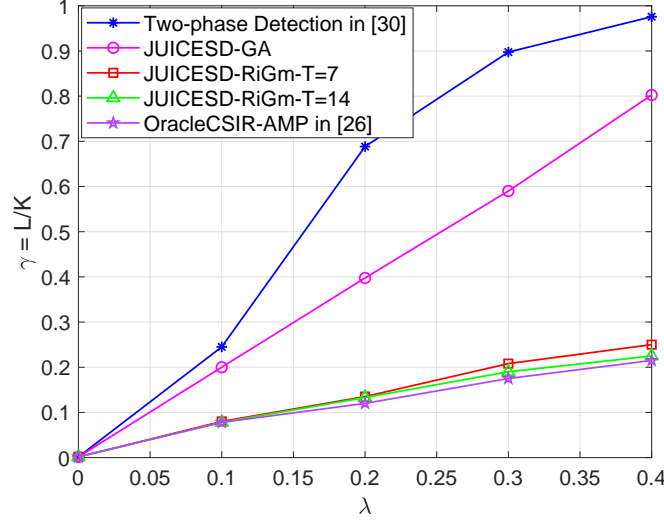


Fig. 7. Phase transition performance with SER threshold $SER_{th} = 10^{-3}$. SNR = 35 dB.

From Fig. 7, the gap between our algorithm and OracleCSIR-AMP increases slightly as λ increases. The reason is that as λ increases, the interference between users increases, which makes the channel estimation difficult. In addition, the gap between our algorithm and OracleCSIR-AMP reduces as the frame length T increases. The reason is that, as T increases, more partially decoded data symbols can be used as pilot to enhance channel estimation in the iterative channel estimation and signal detection process, thereby yielding a better system performance.

C. State Evolution

We evaluate the accuracy of the state evolution of JUICESD-RiGm in this subsection.

1) *Fixed Point*: In Fig. 8(a), we plot the SSD transfer function and the CCE transfer function for JUICESD-RiGm with $\lambda = 0.2$, where the solid line depicts the SSD transfer function for SNR = 30 dB, and the dotted line depicts the CCE transfer function for frame length $T = 7$. The trajectories are obtained by tracking the MSE of the JUICESD-RiGm algorithm in simulations. Here we provide a trajectory example for $T = 7$, SNR = 30 dB. From Fig. 8(a), we see that the simulation trajectory agrees well with the two transfer functions.

2) *Performance Tracking*: Figs. 8(b) and 8(c) show the accuracy of the state evolution in predicting the MSE and SER performance. By defining $\mathbf{g} = [g_1, g_2, \dots, g_K]^T$, we calculate $MSE = \frac{1}{K} \|\mathbf{g} - \hat{\mathbf{g}}\|_2^2$, where $\hat{\mathbf{g}}$ is the estimate of \mathbf{g} given by the JUICESD-RiGm algorithm. We compare the simulated MSE and SER performance with the prediction by the state evolution. From Figs. 8(b) and 8(c), the performance predicted by the state evolution is very close to that by

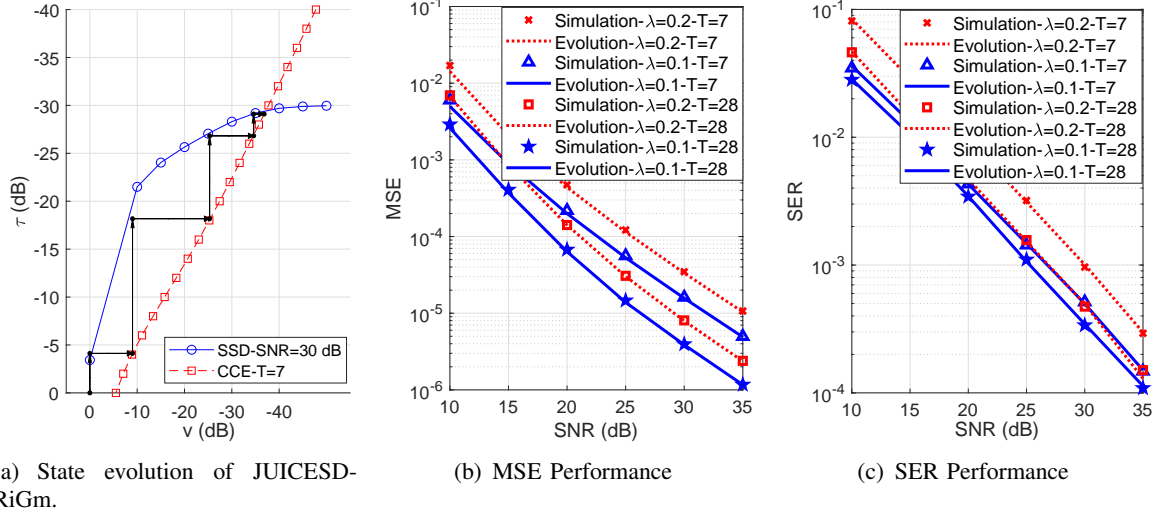


Fig. 8. Performance comparison between SE and simulation; $K = 2000$ and $L = 500$.

simulation. Hence, the state evolution can track the performance of JUICESD-RiGm accurately.

D. Large Scale Fading

In this subsection, we discuss the impact of large scale fading on the system performance. We follow the large scale fading model in [28]. Let d_k denote the distance between user k and the AP. We assume that $\{d_k\}$ are randomly distributed in the range of $[0.05\text{km}, 1\text{km}]$. The path loss model of the wireless channel for user k is given as $\beta_k = -128.1 - 36.7\log_{10}(d_k)$ in dB. The bandwidth of the wireless channel is 1MHz. The power spectral density of the AWGN at the AP is -169dBm/Hz . Fig. 9 shows the SER performance with different user active probabilities. Similar observations as in Section VI-A can be made. This verifies the effectiveness of the proposed JUICESD-RiGm algorithm in a more practical scenario.

VII. CONCLUSIONS AND FUTURE WORKS

We proposed a novel JUICESD framework for mMTC applications. A low-complexity yet near-optimal algorithm named JUICESD-RiGm was developed based on judicious iterative receiver design, sophisticated message passing principles, and accurate rotationally invariant Gaussian mixture message structure. Furthermore, we established the state evolution analysis to predict the performance of JUICESD-RiGm. Numerical results demonstrate that JUICESD-RGMA achieves a significant performance gain over the state-of-the-art algorithms and even outperforms LMMSE receivers with oracle user activity information. The complexity of JUICESD-RiGm is also low; hence it is especially suitable for machine type communications with a massive number

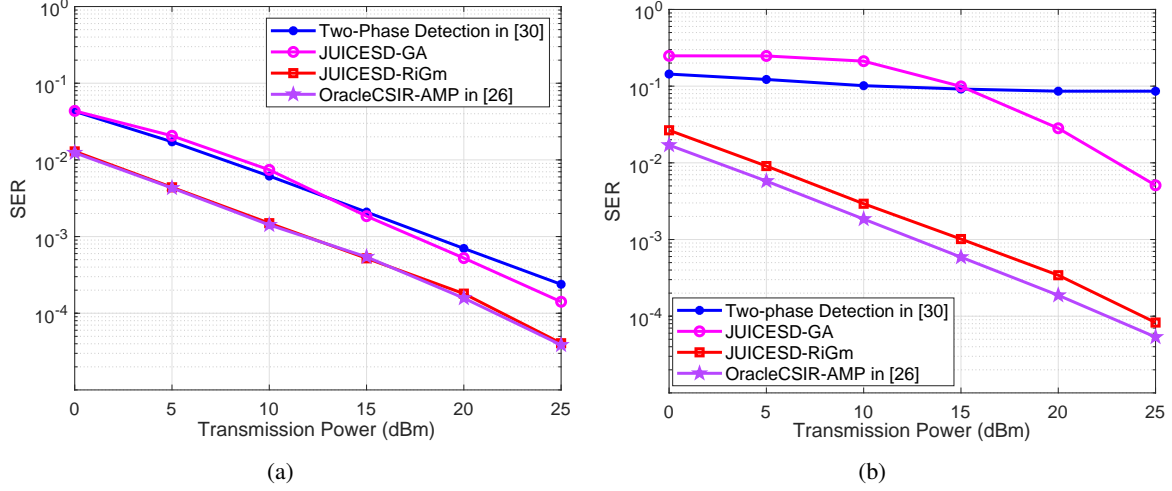


Fig. 9. Performance with large scale fading: $K = 2000$, $L = 500$, $T = 7$. (a) $\lambda = 0.1$ and (b) $\lambda = 0.2$.

of potential devices and short packets. In addition, the performance of JUICESD-RiGm predicted by the state evolution is very close to that by the simulation, which provides insights for future system design and optimization.

This paper focuses only on the single-antenna scenarios. Design of joint detection receiver in the multi-antenna case to support higher transmission rates and a larger number of users can be an interesting extension that will be pursued in our future work.

APPENDIX A: PROOF OF LEMMA 1

We first prove (37a). To this end, it suffices to show $\hat{g}_{k,i'}^{(T'+1)} = \hat{g}_{k,i}^{(T'+1)} e^{j(i'-i)\theta_0}$ for any $i' = 1, \dots, |\Omega_S|$. We note from (35) that if for any $i' = 1, \dots, |\Omega_S|$ and j' satisfying $s_{j'} = s_j e^{j(i'-i)\theta_0}$, the following equalities hold:

$$w_{i',j'}^{(T')} = w_{i,j}^{(T')} \text{ and } \mu_{i',j'}^{(T')} = \mu_{i,j}^{(T')} e^{j(i'-i)\theta_0}, \quad (47)$$

then

$$\hat{g}_{k,i'}^{(T'+1)} = \sum_{j'=1}^{|\mathcal{S}|} w_{i',j'}^{(T')} \mu_{i',j'}^{(T')} = \sum_{j=1}^{|\mathcal{S}|} w_{i,j}^{(T')} \mu_{i,j}^{(T')} e^{j(i'-i)\theta_0} = \hat{g}_{k,i}^{(T'+1)} e^{j(i'-i)\theta_0}. \quad (48)$$

What remains is to verify (47). Recall from (36) that $\hat{g}_{k,i'}^{(T')} = \hat{g}_{k,i}^{(T')} e^{j(i'-i)\theta_0}$. From (34a), we have

$$w_{i',j'}^{(T')} \propto \frac{1}{\pi(v_{g_k}^{(T')} + v_{r_{k,T'+1}}/\|s_{j'}\|^2)} \exp\left(-\frac{\|\hat{g}_{k,i}^{(T')} e^{j(i'-i)\theta_0} - \hat{r}_{k,T'+1}/s_{j'}\|^2}{v_{g_k}^{(T')} + v_{r_{k,T'+1}}/\|s_{j'}\|^2}\right) \quad (49a)$$

$$= \frac{1}{\pi(v_{g_k}^{(T')} + v_{r_{k,T'+1}}/\|s_{j'}e^{j(i-i')\theta_0}\|^2)} \exp\left(-\frac{\|\hat{g}_{k,i}^{(T')} - \hat{r}_{k,T'+1}/(s_{j'}e^{j(i-i')\theta_0})\|^2}{v_{g_k}^{(T')} + v_{r_{k,T'+1}}/\|s_{j'}e^{j(i-i')\theta_0}\|^2}\right) \quad (49b)$$

$$= w_{i,j}^{(T')}. \quad (49c)$$

From (34b), we have

$$\mu_{i',j'}^{(T')} = \frac{\hat{g}_{k,i}^{(T')} e^{j(i'-i)\theta_0} v_{r_{k,T'+1}}/\|s_{j'}\|^2 + v_{g_k}^{(T')} \hat{r}_{k,T'+1}/s_{j'}}{v_{g_k}^{(T')} + v_{r_{k,T'+1}}/\|s_{j'}\|^2} \quad (50a)$$

$$= \frac{\hat{g}_{k,i}^{(T')} v_{r_{k,T'+1}}/\|s_{j'}e^{j(i-i')\theta_0}\|^2 + v_{g_k}^{(T')} \hat{r}_{k,T'+1}/(s_{j'}e^{j(i-i')\theta_0})}{v_{g_k}^{(T')} + v_{r_{k,T'+1}}/\|s_{j'}e^{j(i-i')\theta_0}\|^2} e^{j(i'-i)\theta_0} \quad (50b)$$

$$= \mu_{i,j}^{(T')} e^{j(i'-i)\theta_0}. \quad (50c)$$

Similarly, we can prove (37b). The lemma then readily follows.

REFERENCES

- [1] M. Hasan, E. Hossain, and D. Niyato, "Random access for machine-to-machine communication in LTE-advanced networks: Issues and approaches," *IEEE Commun. Mag.*, vol. 51, no. 6, pp. 86–93, 2013.
- [2] F. Ghavimi and H.-H. Chen, "M2M communications in 3GPP LTE/LTE-A networks: Architectures, service requirements, challenges, and applications," *IEEE Commun. Surveys Tuts.*, vol. 17, no. 2, pp. 525–549, 2014.
- [3] G. Szabo, D. Orincsay, B. P. Gero, S. Gyori, and T. Borsos, "Traffic analysis of mobile broadband networks," in *Proc. WICON*, 2007.
- [4] M. T. Islam, A. E. M. Taha, and S. Akl, "A survey of access management techniques in machine type communications," *IEEE Commun. Mag.*, vol. 52, no. 4, pp. 74–81, 2014.
- [5] N. Xia, H.-H. Chen, and C.-S. Yang, "Radio resource management in machine-to-machine communications – A survey," *IEEE Commun. Surveys Tuts.*, vol. 20, no. 1, pp. 791–828, 2018.
- [6] A. Bayesteh, E. Yi, H. Nikopour, and H. Baligh, "Blind detection of scma for uplink grant-free multiple-access," in *Proc. IEEE Int. Symp. Wireless Commun. Syst. (ISWCS)*, 2014, pp. 853–857.
- [7] L. Dai, B. Wang, Y. Yuan, S. Han, I. Chih-Lin, and Z. Wang, "Non-orthogonal multiple access for 5G: Solutions, challenges, opportunities, and future research trends," *IEEE Commun. Mag.*, vol. 53, no. 9, pp. 74–81, 2015.
- [8] L. Liu, E. G. Larsson, W. Yu, P. Popovski, C. Stefanovic, and E. D. Carvalho, "Sparse signal processing for grant-free massive connectivity: A future paradigm for random access protocols in the Internet of Things," *IEEE Signal Process. Mag.*, vol. 35, no. 5, pp. 88–99, 2018.
- [9] D. Donoho, "Compressed sensing," *IEEE Trans. Inf. Theory*, vol. 52, no. 4, p. 853C857, 2006.
- [10] T. Robert, "Regression shrinkage and selection via the lasso," *J. Roy. Statist. Soc.*, vol. 58, no. 1, pp. 267–288, 1996.
- [11] S. Mallat and Z. Zhang, "Matching pursuits with time-frequency dictionaries," *IEEE Trans. Signal Process.*, vol. 41, no. 12, pp. 3397–3415, 1993.
- [12] J. A. Tropp, "Greed is good: Algorithmic results for sparse approximation," *IEEE Trans. Inf. Theory*, vol. 50, no. 10, pp. 2231–2242, 2004.

- [13] M. Figueiredo, R. Nowak, and S. Wright, "Gradient projection for sparse reconstruction: Application to compressed sensing and other inverse problems," *IEEE J. Sel. Topics Signal Process.*, vol. 1, no. 4, pp. 586–597, 2007.
- [14] D. Needell and J. A. Tropp, "CoSaMP: Iterative signal recovery from incomplete and inaccurate samples," *Appl. Comput. Harmon. Anal.*, vol. 26, no. 3, pp. 301–321, 2009.
- [15] D. L. Donoho, A. Maleki, and A. Montanari, "Message-passing algorithms for compressed sensing," *Proc. Nat. Acad. Sci.*, vol. 106, no. 45, pp. 18 914–18 919, 2009.
- [16] J. Ma, X. Yuan, and P. Li, "Turbo compressed sensing with partial DFT sensing matrix," *IEEE Signal Process. Lett.*, vol. 22, no. 2, pp. 158–161, 2015.
- [17] J. Ma and P. Li, "Orthogonal AMP," *IEEE Access*, vol. 5, no. 99, pp. 2020–2033, 2016.
- [18] S. Rangan, P. Schniter, and A. K. Fletcher, "Vector approximate message passing," in *Proc. IEEE Int. Symp. Inf. Theory (ISIT)*, 2017, pp. 1588–1592.
- [19] Z. Xue, J. Ma, and X. Yuan, "Denoising-based turbo compressed sensing," *IEEE Access*, vol. 5, no. 99, pp. 7193–7204, 2017.
- [20] S. Rangan, "Generalized approximate message passing for estimation with random linear mixing," *arXiv:1010.5141*, 2012.
- [21] S. Rangan, P. Schniter, E. Riegler, A. Fletcher, and V. Cevher, "Fixed points of generalized approximate message passing with arbitrary matrices," *IEEE Trans. Inf. Theory*, vol. 62, no. 12, pp. 7464–7474, 2016.
- [22] J. T. Parker, P. Schniter, and V. Cevher, "Bilinear generalized approximate message passing – Part I: Derivation," *IEEE Trans. Signal Process.*, vol. 62, no. 22, pp. 5839–5853, 2014.
- [23] —, "Bilinear generalized approximate message passing – Part II: Applications," *IEEE Trans. Signal Process.*, vol. 62, no. 22, pp. 5854–5867, 2014.
- [24] M. Bayati and A. Montanari, "The dynamics of message passing on dense graphs, with applications to compressed sensing," *IEEE Trans. Inf. Theory*, vol. 57, no. 2, pp. 764–785, 2011.
- [25] B. Wang, L. Dai, T. Mir, and Z. Wang, "Joint user activity and data detection based on structured compressive sensing for NOMA," *IEEE Commun. Lett.*, vol. 20, no. 7, pp. 1473–1476, 2016.
- [26] C. Wei, H. Liu, Z. Zhang, J. Dang, and L. Wu, "Approximate message passing-based joint user activity and data detection for NOMA," *IEEE Commun. Lett.*, vol. 21, no. 3, pp. 640–643, 2017.
- [27] Y. Zhang, Q. Guo, Z. Wang, J. Xi, and N. Wu, "Block sparse Bayesian learning based joint user activity detection and channel estimation for grant-free NOMA systems," *IEEE Trans. Veh. Technol.*, vol. 67, no. 10, pp. 9631–9640, 2018.
- [28] L. Liu and W. Yu, "Massive connectivity with massive MIMO – Part I: Device activity detection and channel estimation," *IEEE Trans. Signal Process.*, vol. 66, no. 11, pp. 2933–2946, 2018.
- [29] X. Xu, X. Rao, and V. K. N. Lau, "Active user detection and channel estimation in uplink CRAN systems," in *Proc. IEEE ICC*, 2015, pp. 2727–2732.
- [30] G. Hannak, M. Mayer, A. Jung, G. Matz, and N. Goertz, "Joint channel estimation and activity detection for multiuser communication systems," in *Proc. IEEE ICC Workshop*, 2015.
- [31] C. K. Wen, C. J. Wang, S. Jin, K. K. Wong, and P. Ting, "Bayes-optimal joint channel-and-data estimation for massive MIMO with low-precision ADCs," *IEEE Trans. Signal Process.*, vol. 64, no. 10, pp. 2541–2556, 2016.
- [32] Z. Zhang, X. Cai, C. Li, C. Zhong, and H. Dai, "One-bit quantized massive MIMO detection based on variational approximate message passing," *IEEE Trans. Signal Process.*, vol. 66, no. 9, pp. 2358–2373, 2018.
- [33] J. Zhang, X. Yuan, and Y. J. A. Zhang, "Blind signal detection in massive MIMO: Exploiting the channel sparsity," *IEEE Trans. Commun.*, vol. 66, no. 2, pp. 700–712, 2018.
- [34] T. Ding, X. Yuan, and S. C. Liew, "Sparsity learning-based multiuser detection in grant-free massive-device multiple access," *IEEE Trans. Wireless Commun.*, vol. 18, no. 7, pp. 3569–3582, 2019.

- [35] P. Sun, Z. Wang, and P. Schniter, "Joint channel-estimation and equalization of single-carrier systems via bilinear AMP," *IEEE Trans. Signal Process.*, vol. 66, no. 10, pp. 2772–2785, 2018.
- [36] Y. Du, B. Dong, W. Zhu, P. Gao, Z. Chen, X. Wang, and J. Fang, "Joint channel estimation and multiuser detection for uplink grant-free NOMA," *IEEE Wireless Commun. Lett.*, vol. 7, no. 4, pp. 682–685, 2018.
- [37] W. Fan, C. Wen, Y. Wu, J. Ma, and T. A. Tsiftsis, "Message-passing receiver design for joint channel estimation and data decoding in uplink grant-free SCMA systems," *IEEE Trans. Wireless Commun.*, vol. 18, no. 1, pp. 167–181, 2019.
- [38] S. Jiang, X. Yuan, X. Wang, and C. Xu, "Joint user identification, channel estimation, and signal detection for grant-free NOMA," in *Proc. IEEE Globecom*, 2019.